Hippocampal GABA-inhibitory circuitry regulates despair-like behavior in mice

Sang Ho Yoon[1,2], Geehoon Chung[1,4], Woo Seok Song[1,2], Sung Pyo Oh[1], Sang Jeong Kim[1,2], and Myoung-Hwan Kim[1,2,3*]

[1]Department of Physiology and Biomedical Sciences, Seoul National University College of Medicine, Seoul, 03080, Korea. [2]Neuroscience Research Institute, Seoul National University Medical Research Center, Seoul, 03080, Korea. [3]Seoul National University Bundang Hospital, Seongnam, Gyeonggi, 13620, Korea. [4]Present address: Department of Physiology, College of Korean Medicine, Kyung Hee University, Seoul, 02447, Korea.

Running title: Hippocampal E/I balance affects despair

* Correspondence should be addressed to:
Myoung-Hwan Kim
Department of Physiology and Biomedical Sciences, Seoul National University College of Medicine, Seoul, 03080, Korea
Tel: +82-2-740-8377; Fax: +82-2-763-9667; E-mail: kmhwany@snu.ac.kr

Keywords: Hippocampus, Despair, Excitatory/Inhibitory Balance, Antidepressants, Disinhibition, RalBP1

Abstract

Despair is a core symptom of depressive disorders. However, little is known about the neural circuits mediating despair and how they are modified by antidepressants. Here we show that the balance between excitatory and inhibitory neurotransmission (E/I balance) in the hippocampus affects behavioral despair in mice. Reduced interneuron density, knockdown of Gabrg2 or DREADD-mediated suppression of interneuron activity resulted in disinhibition of CA1 neurons and anti-despair-like behaviors in mice. Conversely, pharmacological and chemogenetic potentiation of GABAergic transmission in CA1 neurons rapidly induced despair-like behaviors. Disinhibition induced by the $GABA_AR$ antagonist pentylenetetrazol produced transient antidepressant effects without BDNF elevation in the hippocampus, while ketamine exhibited rapid and sustained antidepressant effects, but the latter was sensitive to the TrkB receptor blocker ANA-12. These results suggest that rapid disinhibition and BDNF-induced long-lasting synaptic modification leads to enhanced E/I balance, which may contribute to acute and sustained behavioral effects of rapid-acting antidepressants.

Introduction

Despair is a common human feeling characterized by the loss of hope that significantly disrupts motivation and goal-directed thinking (Snyder et al., 1991). Notably, despair is one of the core symptoms of depressive disorders, and hopelessness is a strong risk factor for suicidal thoughts (Nestler et al., 2002; Turecki et al., 2012). Although the brain mechanisms underlying despair are unknown, stress is a potent risk factor for depressive symptoms and behavioral despair in humans and laboratory animals, respectively (Nestler et al., 2002; Duman et al., 2016). Conversely, antidepressants improve despair as well as suicidal thoughts in depressed patients and behavioral despair in rodents (Nestler et al., 2002; Duman et al., 2016; Phillips et al., 2019).

A growing body of evidence suggests that rapid-acting antidepressant agents, such as ketamine (an NMDA receptor blocker), the ketamine metabolite (2R,6R)-hydroxynorketamine, and scopolamine (a muscarinic acetylcholine receptor antagonist), share core mechanisms for the synaptic action by rapidly suppressing synaptic inhibition onto pyramidal neurons in the medial prefrontal cortex (mPFC) and hippocampus (Widman and McMahon, 2018; Zanos et al., 2018). Enhanced glutamatergic neurotransmission termed the “glutamate burst” caused by disinhibition of pyramidal neurons is thought to trigger protein synthesis-dependent LTP (long-term potentiation)-like changes in synaptic efficacy and neuronal morphology in the brain areas implicated in the depressive disorder (Duman et al., 2016). Activation of signaling cascades associated with protein synthesis, including eukaryotic elongation factor 2 (eEF2), mammalian target of rapamycin (mTOR), and extracellular signal-regulated kinase (ERK), have been reported to increase BDNF and synaptic protein synthesis and function of neural circuits and mediate the effects of rapid-acting antidepressant agents (Li et al., 2010; Autry et al., 2011; Duman et al., 2016).

A low dose of ketamine or scopolamine is thought to block NMDARs or muscarinic acetylcholine receptors (mAChRs), respectively on GABAergic interneurons. GLYX-13 also increases the excitation/inhibition balance and probability of synaptically driven action potential in hippocampal CA1 neurons through the unknown mechanism (Widman and McMahon, 2018). In line with these findings, L-655,708 or MRK-016, negative allosteric

modulators of α5-subunit-containing GABA A receptor, exhibits a rapid antidepressant activity in rodent models (Fischell et al., 2015). Together these studies demonstrate that disinhibition is associated with the effects of rapid-acting antidepressants. However, it is unclear as to how the disinhibition and the protein synthesis-dependent LTP-like synaptic changes influence behaviors related to depressive disorders.

We previously reported that deficiency of RalBP1, a downstream effector of the small GTP-binding protein RalA and RalB, resulted in reduced interneuron density in the hippocampal CA1 areas (Bae et al., 2013). Basal excitatory synaptic transmission and LTP at the Schaffer collateral-CA1 synapse were normal in RalBP1$^{-/-}$ mice, but long-term depression (LTD) was modestly attenuated (Han et al., 2009). These findings led us to determine whether reduced synaptic inhibition onto CA1 pyramidal neurons caused by reduced interneuron numbers in RalBP1-mutant mice recapitulates disinhibition and the behavioral effects of rapid-acting antidepressants.

While depression- or stress-related synaptic deficits and antidepressant-induced synaptic changes are observed in both mPFC and hippocampus, the behavioral responses to disinhibition of hippocampal CA1 pyramidal neurons are still unclear. To address this issue, we selectively manipulated the activity of CA1 interneurons or inhibitory synaptic transmission onto CA1 pyramidal neurons. We show here that disinhibition of CA1 pyramidal neurons is sufficient to induce anti-despair-like behaviors in mice. The present study also suggest that the acute and long-lasting behavioral effects of the rapid-acting antidepressant ketamine is mediated by rapid disinhibition and BDNF-induced synaptic modification, respectively.

Results

Reduced synaptic inhibition onto CA1 neurons and anti-despair-like behaviors in RalBP1$^{-/-}$ mice

RalBP1 is widely expressed in brain neurons and RalBP1$^{-/-}$ mice exhibit a decreased number of GAD67 (glutamic acid decarboxylase 67)-positive neurons in the hippocampus (Han et al., 2009; Bae et al., 2013). To examine the functional consequence of fewer interneurons in the hippocampal CA1 area, we measured the ratio of synaptic excitation (E) and inhibition (I) onto CA1 pyramidal neurons. We first recorded evoked EPSCs at the reversal potential of IPSCs using a low-chloride (15 mM) pipette solution and then recorded IPSCs at the reversal potential of EPSCs in the same cell (Fig. 1A). The reversal potentials of IPSCs and EPSCs were −57 mV and +3 mV, respectively (Fig. S1). Interestingly, the amplitudes of evoked IPSCs were significantly decreased in RalBP1$^{-/-}$ CA1 neurons (+/+, 920.21 ± 82.42 pA; −/−, 621.43 ± 56.55 pA; $p < 0.05$), whereas evoked EPSCs were not changed (+/+, 190.25 ± 10.94 pA; −/−, 191.02 ± 6.77 pA; $p > 0.05$; Fig. 1B). These results indicate that RalBP1$^{-/-}$ mutation leads to the increased synaptic E/I ratio onto CA1 neurons (Fig. 1C).

Because the hippocampus contains a mixed population of GABAergic (γ-aminobutyric acid-ergic) interneurons derived from medial ganglionic eminence (MGE) and caudal ganglionic eminence (CGE)(Sik et al., 1995; Tricoire et al., 2011), we sought to identify the subtype of interneurons responsible for reduced synaptic inhibition in RalBP1$^{-/-}$ mice. We found fewer MGE-derived parvalbumin (PV)-expressing interneurons but normal density of somatostatin (SOM)-expressing interneurons, which originate from both MGE and CGE, in the RalBP1$^{-/-}$ hippocampal CA1 region (Fig. S2A, B). When we examined the density of CGE-derived interneurons expressing vasoactive intestinal peptide (VIP) and/or cholecystokinin (CCK), fewer VIP-positive interneurons were detected in the RalBP1$^{-/-}$ CA1 area (Fig. S2C, D). However, the density of CCK-positive interneurons was not changed by RalBP1 mutation. These results indicate that altered E/I balance is likely attributable to the reduction of PV- and VIP-positive interneurons.

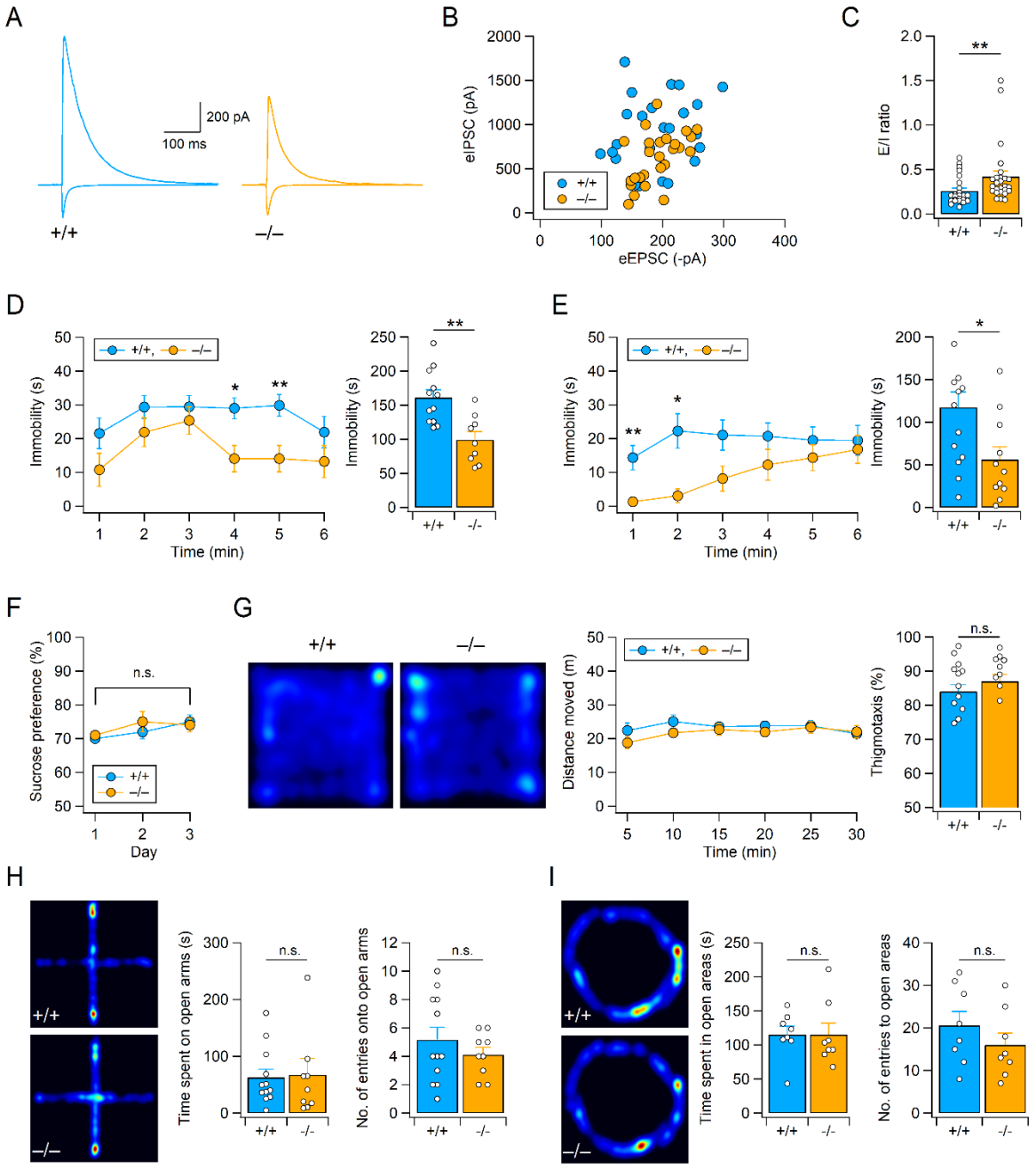

Figure 1. RalBP1$^{-/-}$ mice display decreased synaptic inhibition and anti-despair-like behaviors but normal anxiety levels. (A-C) Enhanced E/I ratio in RalBP1$^{-/-}$ CA1 pyramidal neurons. (A) Representative traces (average of 15 consecutive sweeps) of evoked EPSCs (downward deflections at −57 mV) and IPSCs (upward deflections at +3 mV) recorded in CA1 pyramidal neurons from WT and RalBP1$^{-/-}$ mice. (B) The mean amplitude of evoked IPSCs measured in each cell was plotted against the mean amplitude of EPSCs. (C) The E/I ratios were significantly increased in RalBP1$^{-/-}$ mice. (D, E) RalBP1$^{-/-}$ mice display anti-despair-like behavior. (D) Immobility time of mice was measured every 1 min during the TST (left). Total time spent immobile over 6 min in the TST (right). (E) Forced swimming test (FST) of WT and RalBP1$^{-/-}$ mice (left). RalBP1$^{-/-}$ mice spent significantly less time

immobile during the 6-min FST (right). (F) Preference for sucrose during the 3-day-sucrose-consumption test was not changed in RalBP1$^{-/-}$ mice. (G-I) Normal anxiety levels and locomotor activity in RalBP1$^{-/-}$ mice. (G) Representative activity paths (left), distance moved (middle), and the thigmotaxis levels (right) in the open field test. (H) Representative activity traces (left), time spent in the open arms (middle), and numbers of open-arm entry (right) of WT and KO mice in the elevated plus maze test. (I) Representative activity traces (left), time spent in the open areas (middle), and numbers of entries to open areas (right) of WT and KO mice in the elevated zero-maze test.

To understand the behavioral consequences of reduced synaptic inhibition in RalBP1$^{-/-}$ mice, we first investigated mood-related behaviors in mice. We employed the tail suspension test (TST) to examine depression-like behaviors in RalBP1$^{-/-}$ mice (Steru et al., 1985). Compared to WT control, RalBP1$^{-/-}$ mice spent significantly less time immobile during the 6 min test (Fig. 1D). Consistent with the results from the TST, the genotype-specific difference in the duration of immobility was observed in the forced swim test (FST; Fig. 1E). RalBP1$^{-/-}$ mice spent more time swimming and less time floating than WT littermates in the FST, suggesting that RalBP1 deficiency reduces behavioral despair in mice (Porsolt et al., 1977).

Because behavioral despair is a depression-related endophenotype in mice, we examined whether RalBP1 mutation affects other depression-related behaviors including anhedonia, locomotor activity, and anxiety, using a series of behavioral tests. During the sucrose consumption test, the degree of preference for sucrose was indistinguishable between genotypes (Fig. 1F), indicating that deficiency of RalBP1 does not affect interest in pleasurable activities in mice. RalBP1$^{-/-}$ mice also behaved normally in the open field box (Fig. 1G). This observation excludes the possibility that reduced immobility of RalBP1$^{-/-}$ mice during the both TST and FST might stem from behavioral hyperactivity (Miyakawa et al., 2001). In addition, thigmotaxis (a tendency to remain close to walls) levels of RalBP1$^{-/-}$ mice were not substantially different from those of WT mice (Fig. 1G), indicative of normal anxiety. Normal performance in the both elevated-plus maze and zero maze tests further supports intact anxiety levels in RalBP1$^{-/-}$ mice (Fig. 1H, I). Collectively, these results suggest that the deficiency of RalBP1 selectively affects despair-like behaviors in mice.

Deficiency of RalBP1 does not affect hippocampus-dependent learning, social interaction and sensory gating

Hippocampus plays a critical role in spatial learning and memory processing in rodents. In addition to the reduced interneuron density in the hippocampus, RalBP1 deficiency affects long-term depression (LTD) of excitatory synaptic transmission in CA1 neurons (Han et al., 2009). To determine the cognitive consequences of RalBP1 deficiency, we examined hippocampus-dependent learning behaviors in RalBP1$^{-/-}$ mice. During the 7 days Morris water maze training, control and RalBP1$^{-/-}$ mice exhibited similar escape latency on the hidden platform (Fig. S3A). In accordance with this result, both genotypes spent more time in the target quadrant than any of the three other quadrants in the recall test (Fig. S3B, C). The Morris water maze performance of RalBP1$^{-/-}$ mice was not affected by motor function, as revealed by normal swimming speed (+/+, 16.54 ± 1.29 cm/s; –/–, 17.15 ± 1.37 cm/s; $p > 0.05$, Student t-test) and rotarod performance (Fig. S3D). RalBP1$^{-/-}$ mice also performed normally both in the contextual and in the cued fear conditioning tests (Fig. S3E). These results suggest that hippocampus-dependent learning and memory are intact in RalBP1$^{-/-}$ mice.

Because dysfunction of GABAergic neurotransmission is implicated in the pathophysiology of autism and schizophrenia (Marin, 2012), we assessed social interaction, repetitive behaviors, and sensory gating function in RalBP1$^{-/-}$ mice. In the three-chamber test (Moy et al., 2004), the WT and RalBP1$^{-/-}$ mice showed similar sociability and preference for social novelty. Both genotypes spent more time near a stranger mouse than an inanimate object and preferred a novel stranger mouse to a familiar mouse when an inanimate object was replaced by a novel mouse (Fig. S3F-I). In addition, RalBP1$^{-/-}$ mice did not display repetitive or stereotyped behaviors (Fig. S3J), as determined by normal behaviors in the marble-burying test (Thomas et al., 2009). Impairment in prepulse inhibition of the acoustic startle response, a deficit in sensorimotor gating which is accompanied frequently in the animal models of schizophrenia (Swerdlow et al., 2008), was not detected in RalBP1$^{-/-}$ mice (Fig. S3K). Collectively, these results demonstrate that RalBP1$^{-/-}$ mice do not display autistic or schizophrenia-like behaviors.

Altered hippocampal circuit function is associated with anti-despair-like behavior in RalBP1$^{-/-}$ mice.

We questioned whether a deficiency of RalBP1 accompanies the reduction of interneurons throughout the brain, and whether the change in other brain regions rather than hippocampus is responsible for anti-despair-like behaviors in RalBP1$^{-/-}$ mice. Because the prefrontal cortex and amygdala have been implicated in despair/depression-like behaviors (Covington et al., 2010; Shi et al., 2012; Kumar et al., 2013; Mineur et al., 2014), we examined the density of GABAergic neurons in these brain areas. Intriguingly, the densities of interneurons both in the prefrontal cortex and basolateral amygdala of RalBP1$^{-/-}$ mice were comparable to those of WT mice (Fig. S4).

Because activation of signaling pathways associated with protein synthesis, such as the mammalian target of rapamycin (mTOR), extracellular signal-regulated kinase (ERK) and/or eukaryotic elongation factor 2 (eEF2) signaling pathways, is required for behavioral effects of the rapidly acting antidepressant ketamine (Li et al., 2010; Autry et al., 2011), we investigated whether activation of these signaling pathways is accompanied in the RalBP1$^{-/-}$ hippocampus by measuring the phosphorylation levels of these signaling proteins. RalBP1$^{-/-}$ hippocampus exhibited significantly decreased levels of the phosphorylated (inactivated) form of eEF2 compared to the WT hippocampus, whereas both genotypes showed similar levels of total eEF2 in the hippocampus (Fig. 2A). Since the dephosphorylation (activation) of eEF2 stimulates protein synthesis and the blockade of action potential-mediated network activity promotes phosphorylation of eEF2 (Sutton et al., 2007; Autry et al., 2011), enhanced hippocampal network activity caused by disinhibition promotes dephosphorylation of eEF2 and translation of downstream signaling molecules such as brain-derived neurotrophic factor (BDNF)(Autry et al., 2011). However, hippocampal BDNF levels in RalBP1$^{-/-}$ mice were not significantly different from WT littermates. Consistent with this result, modification of mTOR and ERK signaling, downstream pathways of BDNF-TrkB (tropomyosin receptor kinase B) signaling, was not detected in the RalBP1$^{-/-}$ hippocampus, as neither total protein expression nor phosphorylation levels were different between genotypes (Fig. 2A). Considering that excitatory synaptic function including NMDAR- and AMPAR-mediated synaptic transmission as well as expression levels of excitatory synaptic proteins is normal in RalBP1$^{-/-}$ hippocampus (Han et

al., 2009), activation of the eEF2 signaling pathway in the hippocampus might be associated with reduced synaptic inhibition in RalBP1$^{-/-}$ mice. These findings further indicate that disinhibition of principal neurons, without the blockade of NMDAR or BDNF elevation, is sufficient for the activation of eEF2 signaling in the hippocampus and behavioral anti-despair.

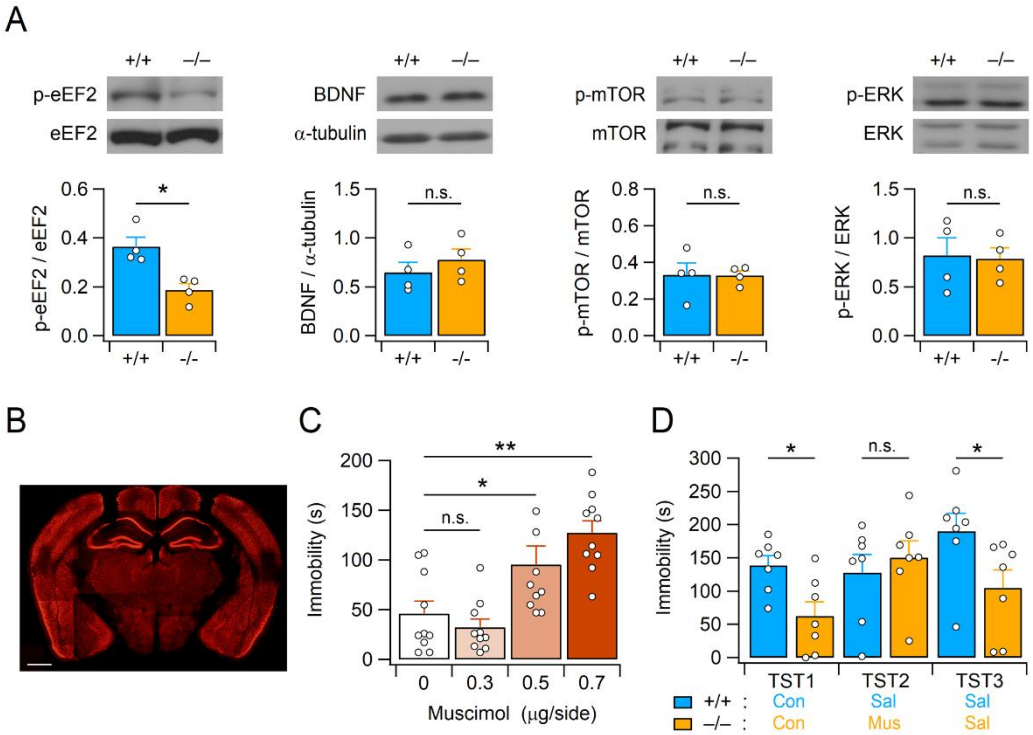

Figure 2. Altered hippocampal eEF2 signaling and attenuation of anti-despair-like behavior by intrahippocampal infusion of muscimol in RalBP1$^{-/-}$ mice. (A) Representative western blot images (top) and quantification (bottom) showing enhanced eEF2 activation but normal BDNF, mTOR, and ERK signaling in the RalBP1$^{-/-}$ hippocampus. The blots were cropped and full blots are presented in Supplementary Figure S9. Western blotting using anti-α-tubulin antibody was performed to ensure equal protein loading and transfer, and quantification of BDNF levels in each sample. (B) Representative image showing the cannula placement in the mouse brain for muscimol infusion. The section was immunostained with anti-NeuN antibodies. Scale bar, 1 mm. (C) Hippocampal infusion of muscimol increases TST immobility time in a dose-dependent manner. (D) Potentiation of GABAergic transmission in the hippocampal CA1 area reverts anti-despair-like behavior of RalBP1$^{-/-}$ mice. TST was performed 30 min after completion of infusion and inter-test intervals were 2 days.

Based on the observation of altered hippocampal network and anti-despair-like behaviors in RalBP1$^{-/-}$ mice, we questioned if pharmacological potentiation of GABAergic transmission in the hippocampal CA1 area would induce despair-like behavior in mice. Indeed, bilateral infusion of muscimol, a $GABA_A$ receptor agonist, into the dorsal hippocampal CA1 region of

WT mice induced despair-like behaviors in a dose-dependent manner during the TST (Fig. 2B, C). We further determined whether enhancement of GABAergic transmission in the CA1 area would reverse anti-despair-like behavior in RalBP1$^{-/-}$ mice. Cannula implantation did not affect anti-despair-like behaviors in RalBP1$^{-/-}$ mice, as we again observed reduced immobility of RalBP1$^{-/-}$ mice during the TST (Fig. 2D, TST1). However, when muscimol (0.5 μg) was infused bilaterally into the CA1 region of RalBP1$^{-/-}$ hippocampus, immobility of RalBP1$^{-/-}$ mice was comparable to that of saline-treated WT mice (Fig. 2D, TST2). Behavioral changes in RalBP1$^{-/-}$ mice were treatment specific because RalBP1$^{-/-}$ mice regained anti-despair-like behaviors when both genotypes of mice received saline (Fig. 2D, TST3). These results indicate that altered hippocampal network activity might be responsible for anti-despair-like behaviors in RalBP1$^{-/-}$ mice.

Suppression of synaptic inhibition onto CA1 pyramidal neurons induces anti-despair-like behavior

Synaptic GABA A receptors ($GABA_A$Rs) contain one of the three γ subunits ($\gamma_1 - \gamma_3$), and γ_2 subunit encoded by the Gabrg2 gene plays a critical role in clustering major postsynaptic $GABA_A$Rs (Essrich et al., 1998; Jacob et al., 2008). To examine the direct causal relationship between reduced synaptic inhibition in CA1 neurons and anti-despair-like behaviors of mice, we prepared four different knockdown vectors containing short hairpin RNA (shRNA) targeting $GABA_A$R γ_2 subunit (Gabrg2), and determined the gene knockdown efficiency of each construct in HEK293T cells (Fig. S5). To interfere with Gabrg2 expression in CA1 neurons, an shRNA sequence having the highest target knockdown activity (Gabrg2-shRNA#3, shGabrg2) was subcloned into the lentiviral transfer vector and virally delivered into the CA1 neurons (Fig. 3A, B). Indeed, inhibitory synaptic transmission was attenuated by Gabrg2 knockdown. Gabrg2 knockdown significantly decreased the frequency but not the amplitude of miniature inhibitory postsynaptic currents (mIPSCs) in CA1 neurons, indicating that Gabrg2 knockdown reduces the number of functional GABAergic synapses (Fig. 3C-E). In contrast to mIPSCs, neither the frequency nor the amplitude of miniature excitatory postsynaptic currents (mEPSCs) was affected by Gabrg2 knockdown (Fig. 3F-H).

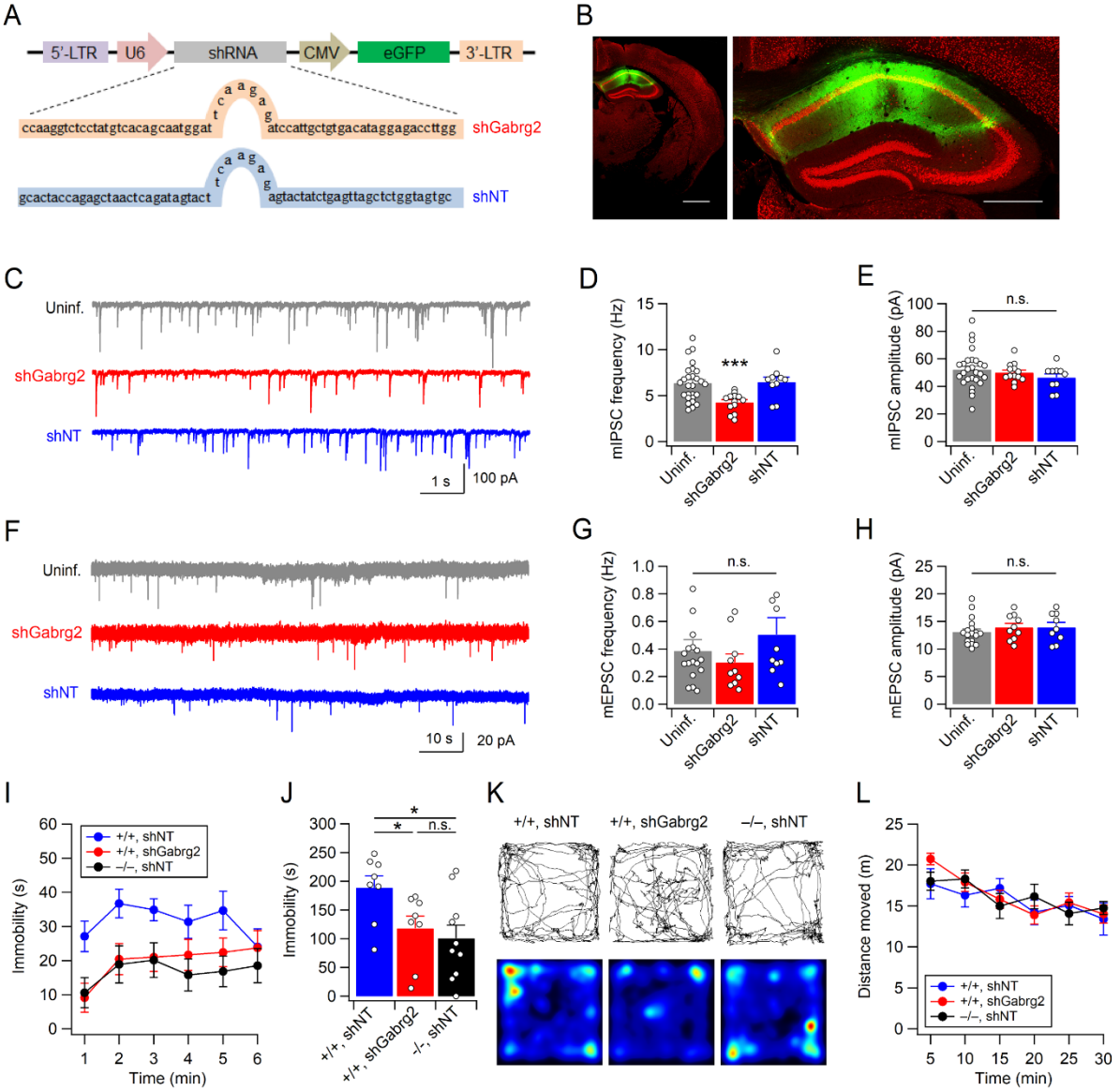

Figure 3. Knockdown of Gabrg2 in hippocampal CA1 neurons reduces despair-like behaviors. (A) Schematic diagram of the viral genome expressing Gabrg2-shRNA#3 (shGabrg2) or non-targeting shRNA (shNT). (B) Coronal brain section from mice expressing eGFP (green) in the hippocampal CA1 area (left). Sections were co-stained with the neuronal marker NeuN (red). Right, enlarged image of the hippocampal area. Scale bars, 1 mm (left) and 500 μm (right). (C) Sample traces of mIPSCs recorded in CA1 pyramidal neurons infected with virus expressing shGabrg2 or NT, and nearby uninfected (uninf.). (D) Gabrg2 knockdown reduces the frequency of mIPSCs. (E) Summary of the mean amplitudes of mIPSCs obtained from uninfected and virus-infected (shGabrg2 or shNT) CA1 neurons. (F-H) Gabrg2 knockdown had no effect on mEPSCs. Sample traces (F), mean frequencies (G) and mean amplitudes (H) of mEPSCs recorded in CA1 pyramidal neurons infected with virus expressing shGabrg2 or NT, and nearby uninfected. (I) shRNA-mediated suppression of Gabrg2 expression in hippocampal CA1 neurons reduces immobility of mice in the TST. (J) Summary of time spent immobile in each experimental group during the 6 min-TST. (K) Representative images showing exploration path during the first 5 min (top) and entire 30-min period (bottom) in the open field test. (L) Quantification of distance moved in the open field box.

These results rule out nonspecific neuronal defects induced by shRNA expression or lentivirus infection, and also exclude homeostatic downregulation of glutamatergic neurotransmission which is observed in Gabrg2 mutant mice (Ren et al., 2016). Normal mIPSCs and mEPSCs in CA1 neurons expressing a non-targeting shRNA (shNT) further support the specificity of Gabrg2 knockdown. We next examined the effect of Gabrg2 knockdown in CA1 neurons on despair-like behaviors. Similar to RalBP1$^{-/-}$ mice injected with virus expressing shNT, WT mice infected with shGabrg2-expressing virus spent significantly less time immobile in the TST than those infected with shNT virus (Fig. 3I, J). Given that general locomotor activities in the open field box were not changed by Gabrg2 knockdown in CA1 neurons (Fig. 3K, L), reduced immobility in the TST reflects anti-despair-like behavior in mice.

Activity of CA1 interneurons modulates behavioral despair in mice

Reduction of CA1 interneurons or inhibitory synaptic transmission onto CA1 pyramidal neurons induced anti-despair-like behaviors in mice. These findings led us to hypothesize that changes in CA1 interneuron activity might modulate behavioral despair. To selectively manipulate the activity of CA1 interneurons, we expressed excitatory (hM3Dq) or inhibitory (hM4Di) designer receptors exclusively activated by designer drugs (DREADDs) using adeno-associates virus (AAV) carrying Cre-dependent (double-floxed inverse orientation, DIO) DREADD receptor expression vectors (Fig. 4A). When AAV2-hSyn-DIO-DREADDs-mCherry were stereotaxically injected into the hippocampal CA1 area of Vgat-ires-Cre knock-in (Vgat-Cre) mice, mCherry signals were restricted to GAD67-positive inhibitory neurons (Fig. 4B), including PV- and SST-expressing neurons (Fig. S6). To confirm the action of clozapine-N-oxide (CNO) in controlling the activity of DREADD-expressing neurons, we examined the effect of CNO on the membrane potential and spontaneous firing of these neurons in hippocampal slices using whole-cell patch clamp recordings. Bath application of CNO rapidly depolarized the membrane potential and significantly increased the firing rate in hM3Dq-expressing neurons, whereas hM4Di-expressing neurons exhibited hyperpolarization and decreased firing rate in response to CNO perfusion (Fig. 4C-E). In the absence of DREADDs (DiO-mCherry), CNO had no effect either on the membrane potential or firing rate.

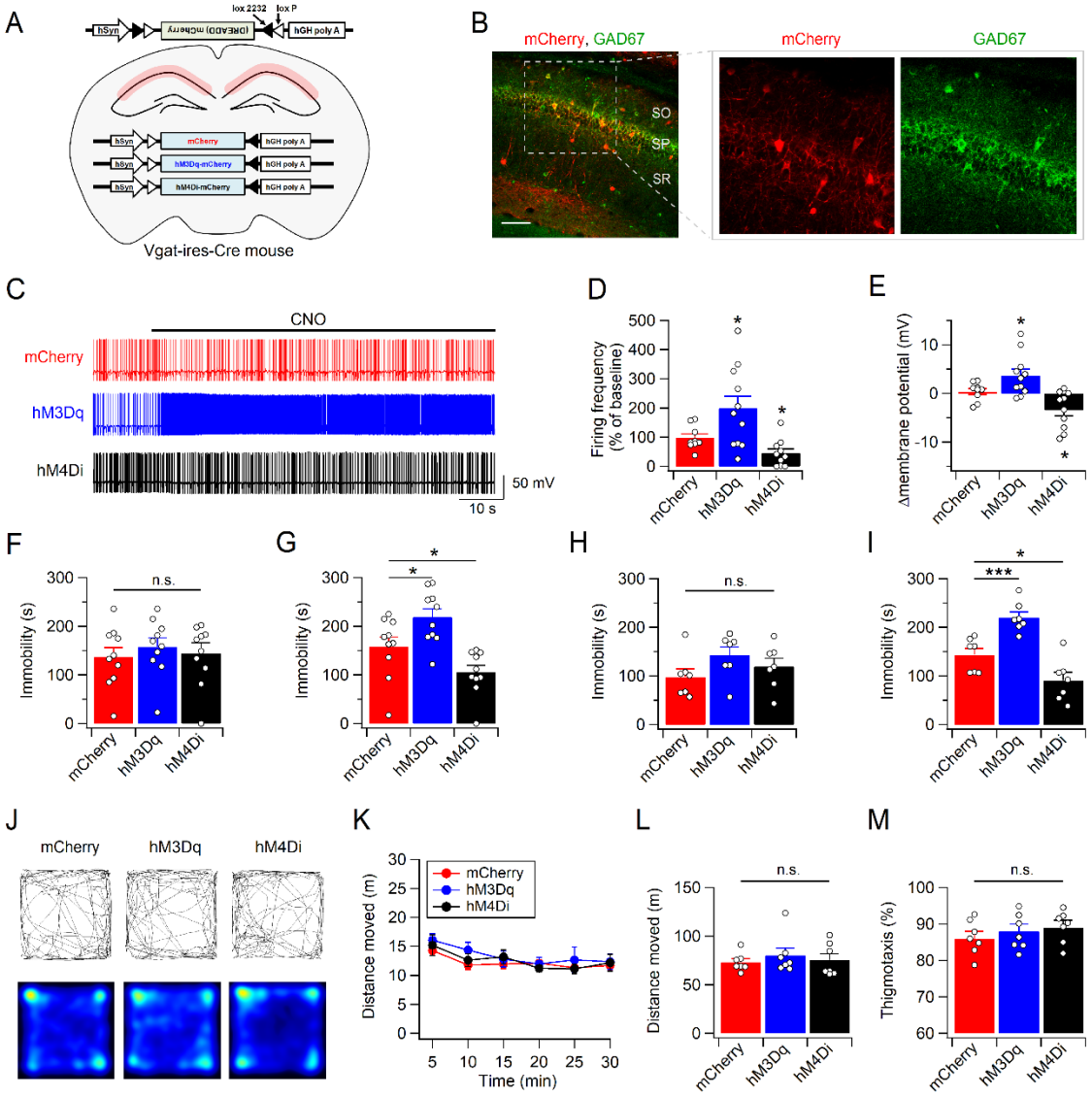

Figure 4. Pharmacogenetic manipulation of CA1 interneurons alters behavioral despair. (A) Design of Cre-dependent expression of mCherry, hM3Dq-mCherry or hM4Di-mCherry in the CA1 interneurons. (B) Double immunostaining of hippocampal sections with mCherry (red) and GAD67 (green) antibodies revealed interneuron-specific expression of mCherry in the CA1 subfield of Vgat-Cre mice. Scale bar, 100 μm. SO, stratum oriens; SP, stratum pyramidale; SR, stratum radiatum. (C) Representative voltage traces recorded from interneurons expressing mCherry, hM3Dq-mCherry or hM4Di-mCherry before and during the bath application of CNO (5 μM). (D, E) Quantification of the CNO effects on firing rate (D) and membrane potential (E). (F-I) Bar graphs represent total time spent immobile during the TST (F, G) and FST (H, I). In the absence of CNO, the DREADD expression did not affect despair-like behaviors in the TST (F) and FST (H). CNO-induced activation or suppression of CA1 interneurons expressing DREADDs bidirectionally modifies immobility time in the TST (G) and FST (I). CNO was administered 30 min before the test. (J) Sample path recordings during the first 5 min (top) and entire 30-min period (bottom) in the open field test. (K) The open field activities of the control (mCherry) and DREADD-expressing mice with 5-min intervals measured 30 min after CNO injection. (L, M) Quantification of the total distance moved (L) and thigmotaxis (M) in the open field box.

We next explored the role of CA1 interneuron activity in modulating behavioral despair (Fig. 4F-I). The expression of DREADDs in inhibitory neurons did not affect behavioral despair. All groups spent a similar amount of time immobile during the both TST (Fig. 4F) and FST (Fig. 4H) in the absence of CNO. Interestingly, CNO injection markedly increased the immobility time of hM3Dq-expressing mice in the TST (Fig. 4G) and FST (Fig. 4I). In accordance with this observation, hM4Di-expressing mice exhibited reduced immobility in the both TST and FST in response to CNO injection. However, CNO injection did not produce any statistically significant changes in immobility time of mCherry-expressing mice (TST: $t_{(18)} = -0.726$, $p = 0.487$; FST: $t_{(12)} = -2.442$, $p = 0.054$). Importantly, we found that CNO-induced changes in TST and FST behaviors did not stem from altered general activity or anxiety, because hM3Dq- and hM4Di-expressing mice showed similar locomotor activities and thigmotaxis levels to mCherry-expressing mice in the open field test (Fig. 4J-M). Collectively, these results indicate that the change in CA1 interneuron activity is sufficient for the modulation of behavioral despair.

Pharmacological disinhibition induces rapid eEF2 activation in the hippocampus and transient antidepressant behavior

RalBP1$^{-/-}$ mice exhibit enhanced eEF2 activation in the hippocampus (Fig. 2), but expression levels and function of NMDAR in RalBP1$^{-/-}$ CA1 neurons are intact (Han et al., 2009). Based on these observations, we hypothesized that disinhibition without NMDAR inhibition might be sufficient to activate eEF2 signaling. To test this possibility, we examined the effect of the $GABA_AR$ antagonist pentylenetetrazol (Huang et al., 2001) on phosphorylation and expression levels of eFF2 in the WT hippocampus (Fig. 5A). Unexpectedly, a single administration of a subconvulsive dose (20 mg/Kg, i.p.) of pentylenetetrazol (PTZ) induced rapid (< 30min) and significant dephosphorylation of eEF2 in the hippocampus. We questioned whether the PTZ-induced activation of eEF2 causes elevation of BDNF in the hippocampus. However, changes in BDNF levels and the activation of mTOR and ERK signaling were not detected in the hippocampal extracts (Fig. 5A). These results imply that the NMDAR blockade is not essential for the activation of eEF2 in the hippocampus in vivo, and that eEF2 dephosphorylation does not necessarily lead to enhanced BDNF production.

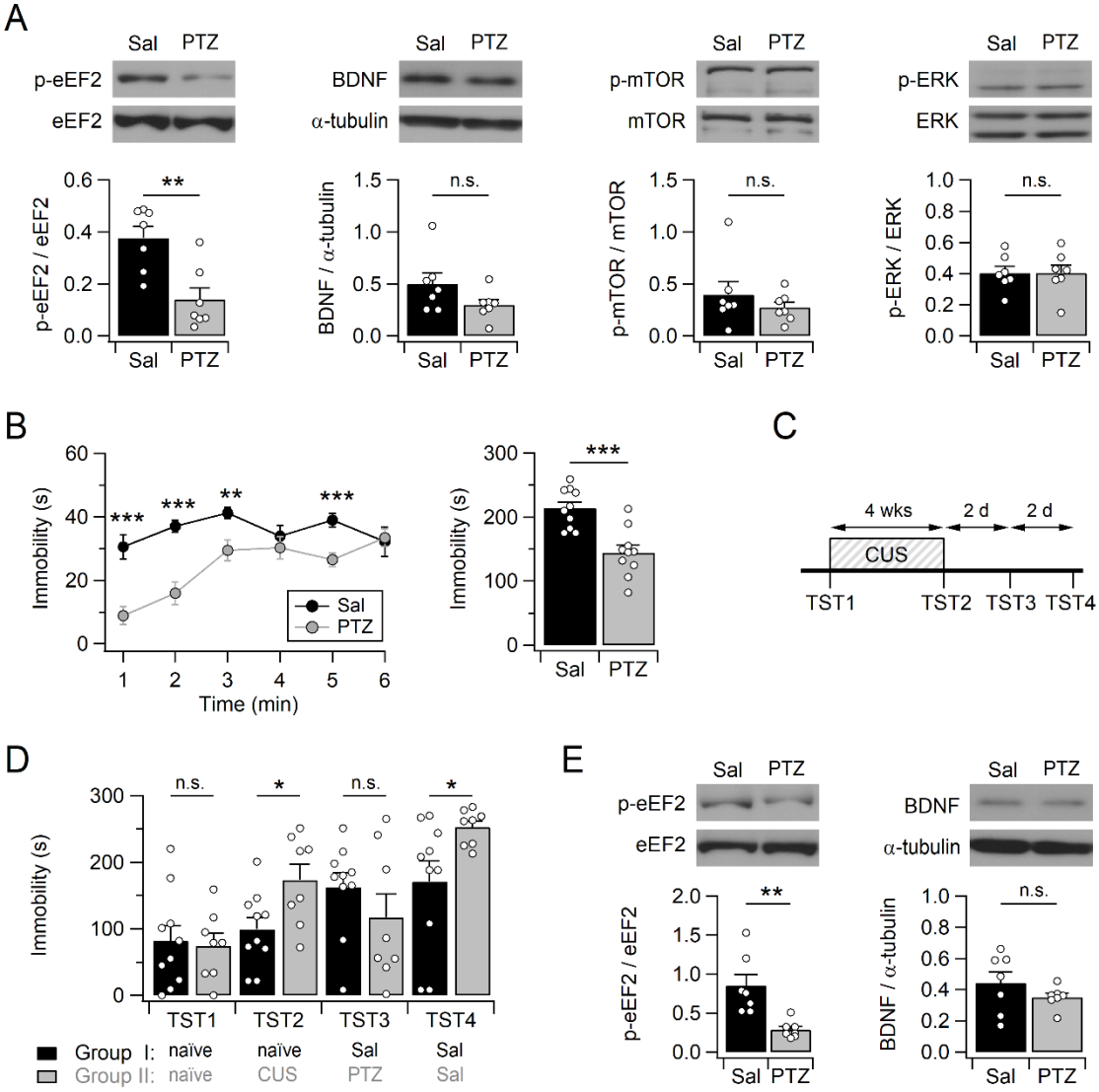

Figure 5. PTZ injection induces rapid and sustained eEF2 dephosphorylation in the hippocampus but transient antidepressant effects. (A) Representative western blots for total and phosphorylated forms of eEF2, mTOR and ERK, and BDNF in hippocampal samples obtained 30 min after treatment (top). Densitometric analysis shows selective effect of PTZ on eEF2 but not BDNF, mTOR and ERK signaling in the hippocampus (bottom). (B) Mice received PTZ exhibit reduced immobility during the TST. Bar graph represents total immobility time over 6 min (right). TST was performed 30 min after PTZ injection. (C) Experimental scheme. After scoring immobility time of naïve WT mice in the TST (TST1), one group of mice were exposed to CUS for 4 weeks. CUS-induced despair-like behaviors were analyzed by the TST (TST2) on the next day after the end of CUS. Thirty minutes before the third TST (TST3), control and stressed mice received saline and PTZ, respectively. Both groups of mice were injected with saline 30 min before the fourth TST (TST4). (D) PTZ administration transiently reduced despair-like behaviors induced by CUS. (E) Single PTZ administration induced a sustained activation of eEF2 signaling in the hippocampus. Representative western blots for eEF2 and BNDF in hippocampal lysates prepared 48 h after PTZ injection (top). Quantification of p-EF2/EF2 ratio and BDNF levels in the hippocampus (bottom). (A, E) The blots were cropped and full blots are presented in Supplementary Figure S9.

However, when we examined the effect of acute PTZ administration on TST behaviors using different cohorts of mice, a single administration of PTZ (20 mg/Kg, i.p.) significantly reduced immobility time of mice during the 6-min TST (Fig. 5B). This concentration of PTZ is a sub-convulsant dose because we did not observe any detectable convulsions, seizure behaviors or hyperactivities (Fig. S7).

We further examined the effect of PTZ-induced disinhibition on stress-induced despair-like behaviors. To this end, we measured the immobility time of WT mice in the TST (TST1; Fig. 5C, D), and assigned the mice to two experimental groups. One of the groups received chronic unpredictable stress (CUS) for 4 weeks (Fig. 5C). When we compared TST behaviors of the two groups after the end of CUS, mice exposed to CUS spent significantly more time immobile compared to controls, indicating CUS-induced despair-like behaviors in the stressed group (TST2; Fig. 5D). Acute PTZ administration (20 mg/Kg, i.p., 30 min before the test) was also effective to improve despair-like behaviors of the stressed mice, as both groups of mice spent similar amount of time immobile in the third TST (TST3; Fig. 5D). Intriguingly, a single PTZ administration did not induce a long-lasting behavioral change in the stressed mice. Mice exposed to chronic stress displayed enhanced despair-like behavior compared to control mice in the fourth TST that was performed two days after PTZ administration (Fig. 5D). Because PTZ has a short half-life (2.5 – 3.8 h) in rodents (Meilleur et al., 2003), the rapid and short-lasting behavioral effect of PTZ might be due to transient synaptic disinhibition and activation of eEF2. We then asked whether the activity of eEF2 would return to the basal level within 2 days after PTZ administration. To explore this question, we injected PTZ into a different cohort of unstressed mice, and investigated the phosphorylation levels of eEF2 in the hippocampus and TST behaviors of mice 48 h after the drug administration. Unexpectedly, phosphorylation levels of eEF2 were still lower in the PTZ-group than the vehicle-group, indicating that activation of eEF2 lasted for 48 h after PTZ injection (Fig. 5E). Moreover, despite the sustained eEF2 activation, BDNF levels in the hippocampus did not increased in response to systemic injection of PTZ. Similar to mice exposed to CUS, antidepressant behavior induced by a single administration of PTZ did not persist for 48 h in unstressed mice (Fig. S8). These findings further indicate that activation of eEF2, in the absence of disinhibition and BDNF elevation, is not sufficient to induce antidepressant behaviors.

Activation of BDNF signaling is critical for sustained antidepressant effect of ketamine

Because ketamine exhibits rapid and long-lasting antidepressant effects, we compared the effects of ketamine on TST behaviors and intracellular signaling with those of PTZ. In contrast to PTZ, the behavioral effect of ketamine (5 mg/kg, i.p.) persisted for more than 48 h after single intraperitoneal administration (Fig. 6A). We questioned whether the reduced immobility at 30 min after dosing originated from dissociative effects of ketamine (Zanos et al., 2016). However, when we examined the effects of ketamine on the open-field activity of mice using independent cohorts of animals, enhanced locomoter activities did not last for more than 10 min (Fig. 6B, C). This observation indicates that the decreased immobility during the TST at 30 min after administration unlikely stemmed from hyperlocomotion or side-effects of ketamine.

We next investigated the effect of ketamine on intercellular signaling at 30 min after single administration using a different cohort of mice. Ketamine showed similar effects with PTZ on eEF2 in the hippocampus, whereas BDNF levels were selectively changed by ketamine (Fig. 6D). Ketamine (5 mg/kg, i.p.) rapidly increased the mature isoform of BDNF (m-BDNF) in the hippocampus. Notably, phosphorylation of mTOR and ERK in the hippocampus was significantly enhanced within 30 min of ketamine administration (Fig. 6E), indicating the activation of downstream signaling pathways of BDNF. If the activation of BDNF signaling was associated with the long-lasting antidepressant effects of ketamine, suppression of BDNF downstream pathways would preferentially impair the sustained effect of ketamine leaving the transient effect intact. Because the m-BDNF exhibits higher affinity for the tyrosine kinase B (TrkB) receptor than the p75 neurotropin receptor, and cellular effects of m-BDNF are mainly mediated by the TrkB receptor (Huang and Reichardt, 2001; Kowianski et al., 2018), we analyzed the effect of TrkB receptor inhibition on antidepressant effects of ketamine. The TrkB receptor antagonist ANA-12 penetrates the blood-brain barrier and reaches peak concentration in the mouse brain as early as 30 minutes after the intraperitoneal injection (Cazorla et al., 2011). We therefore pretreated mice with ANA-12 (0.5 mg/kg, i.p) 30 min before ketamine injection and tested TST behaviors both 30 min and 48 h after ketamine treatment (Fig. 6F). Ketamine still exhibited antidepressant effect on ANA-12 pretreated mice at 30 min after treatment such that immobility time during the TST was significantly reduced by ketamine.

This finding is consistent with previous results that pretreatment (30 min) with intracerebroventricular administration of K252a, another TrkB receptor antagonist, did not block antidepressant effect in the TST at 30 min after ketamine treatment (Koike et al., 2013). Surprisingly, the antidepressant effects of ketamine did not persist for 48 h in ANA-12 pretreated mice (Fig. 6F). Both groups spent a similar amount of time immobile in the TST at 48 h after saline or ketamine injection. These results imply that enhanced BDNF levels and the activation of downstream signaling pathways are responsible for the long-lasting antidepressant effect of ketamine (Shirayama et al., 2002; Duman and Monteggia, 2006; Autry et al., 2011).

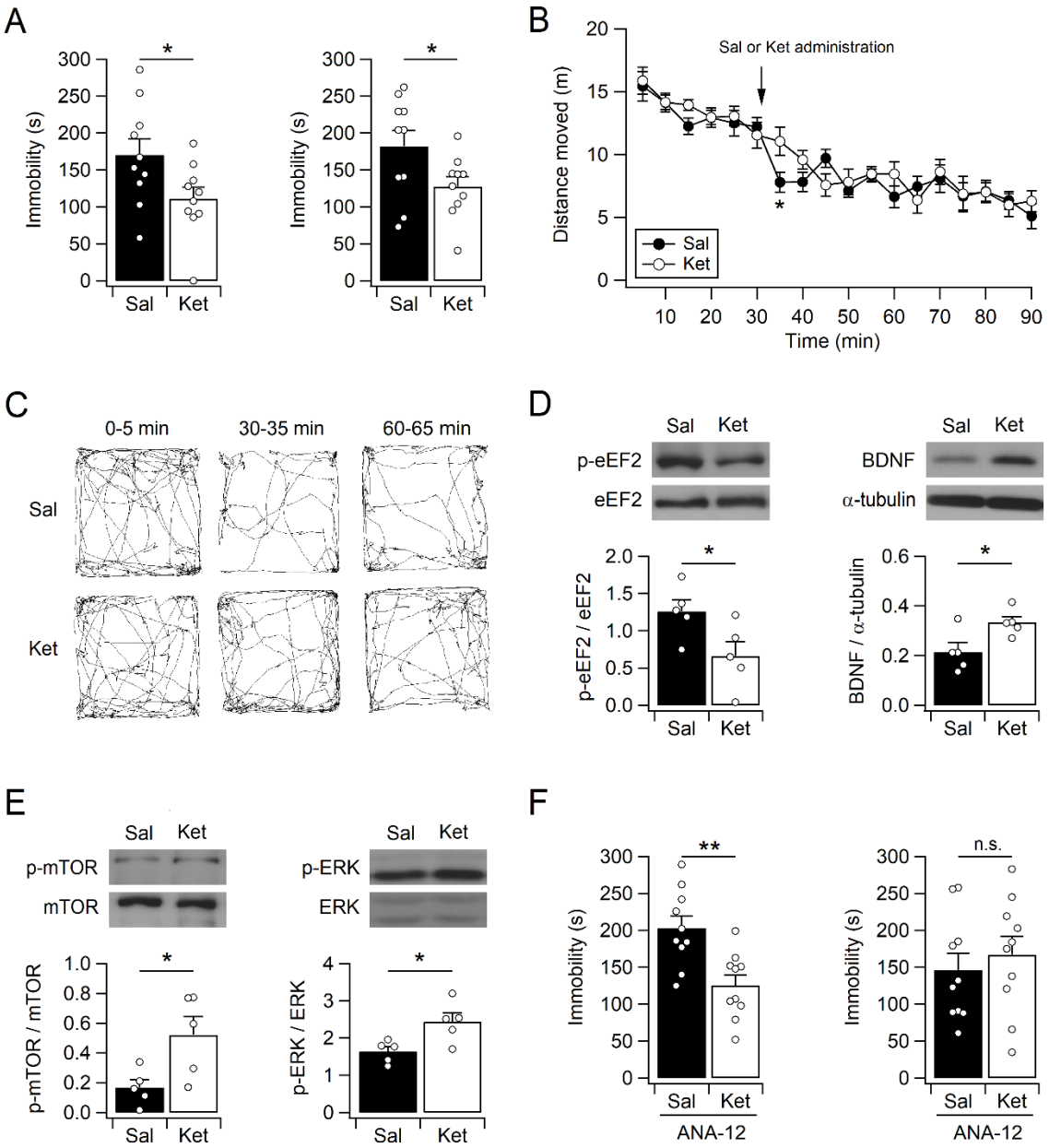

Figure 6. Long-lasting but not rapid antidepressant effects of ketamine require BDNF-TrkB signaling. (A) Single ketamine (Ket) injection induces rapid and long-lasting antidepressant effects. Reduced immobility in the TST was observed at both 30 min (left) and 48 h (right) after ketamine injection. (B) Open field activities of mice in 5-min time bins across a 90-min session. Mice received ketamine (5 mg/kg) or saline (Sal) 30 min after baseline activity recording. (C) Sample path recordings during the first 5 min, and immediate after (30-35 min) and 30 min after (60-65 min) drug administration. (D, E) Ketamine rapidly activate eEF2, BDNF, mTOR and ERK signaling pathways in the hippocampus. Representative western blots (top) and quantification (bottom) of the proteins in hippocampal lysates obtained 30 min after ketamine injection. (F) Pretreatment (30 min before ketamine injection) of ANA-12 blocks sustained but not acute antidepressant effects of ketamine. Bar graphs represent time spent immobile of mice during the 6 min-TST performed 30 min (left) and 48 h (right) after ketamine injection.

Discussion

The present study shows that the balance between the excitatory and inhibitory synaptic transmissions (E/I balance) in the hippocampal network affects despair-like behaviors in mice. RalBP1 mutant mice exhibit anti-despair-like behaviors and reduced synaptic inhibition with normal excitatory synaptic transmission in the hippocampus. Reduced despair-like behaviors of RalBP1$^{-/-}$ mice were reversed by pharmacological potentiation of the inhibitory synaptic transmission in CA1 neurons. In addition, hippocampal CA1-specific suppression of inhibitory synaptic transmission by virus-mediated knockdown of Gabrg2 in WT mice recapitulated anti-despair-like behaviors of RalBP1 mutant mice. Similarly, chemogenetic manipulation of CA1 interneuron activity modified despair-like behaviors in mice without affecting general locomotor activity and anxiety. Thus, the E/I balance in the hippocampal network affects behavioral despair. Our study also provides experimental evidence showing that BDNF signaling is critical for the long-lasting behavioral effect of ketamine.

Based on the anatomic connectivity and deficit-lesion studies, it is widely accepted that the hippocampus is functionally segregated along the hippocampal longitudinal axis; dorsal (posterior in primates) and ventral (anterior in primates) regions of hippocampus contribute to cognitive and emotional processing, respectively (Moser and Moser, 1998; Fanselow and Dong, 2010; O'Leary and Cryan, 2014; but see Strange et al., 2014). Although the brain area responsible for despair is still unclear, recent studies support our observation that dorsal hippocampal network activity affects depression-related behaviors, at least despair-like behaviors in rodents. Suppression of dendritic expression of hyperpolarization-activated cyclic nucleotide-gated (HCN) channels in CA1 neurons of the dorsal hippocampus enhanced neuronal excitability, while behavioral despair was decreased (Kim et al., 2012). Restoration of HCN channel function by viral expression of TRIP8b in CA1 pyramidal neurons of the dorsal hippocampus reversed neuronal excitability and anti-despair-like behaviors in TRIP8b mutant mice (Han et al., 2017). Considering that neural network activity is determined by synaptic function and cellular excitability, it is plausible that reduced synaptic inhibition and enhanced neuronal excitability similarly influence neural network activity. In agreement with this idea, we observed that bilateral infusion of muscimol (a potent, selective agonist of the $GABA_A$Rs) into the dorsal hippocampal CA1 area increased immobility of WT mice in a dose-

dependent manner, and reversed anti-despair behaviors of RalBP1$^{-/-}$ mice during the TST (Fig. 2). Although the circuit mechanisms are not fully understood, previous studies have shown that pharmacological manipulations of the dorsal hippocampus modified despair behaviors in rodents. Stereotaxic infusion of UFP-101 (the nociceptin/orphanin-FQ opioid peptide receptor antagonist), 1-aminocyclopropanecarboxylic acid (a partial agonist at strychnine-insensitive glycine receptors associated with the NMDAR complex), CGP 37849 (a competitive NMDA receptor antagonist) and imipramine (a tricyclic antidepressant) into the dorsal hippocampus induced anti-despair-like behaviors (Przegalinski et al., 1997; Goeldner et al., 2010). Mice deficient for cannabinoid type 1 receptor (CB1) exhibited decreased BDNF levels in the hippocampus and increased despair behavior in the tail suspension test. Enhanced despair behavior of CB1-mutant mice was reversed by the local administration of BDNF into the dorsal hippocampus (Aso et al., 2008). Similarly, a single bilateral infusion of BDNF into the dentate gyrus or CA3 of dorsal hippocampus reduced despair-like behaviors in rats without affecting locomotor activity and anxiety (Shirayama et al., 2002). Thus, in addition to cognitive processing, the dorsal hippocampus seems to affect despair-like behaviors rather than anxiety or anhedonia. Considering that mPFC neurons have direct synaptic connections with axon terminals of CA1 neurons from both dorsal and ventral hippocampi (Xu and Sudhof, 2013; Ahrlund-Richter et al., 2019), it is possible that dorsal hippocampal projections to mPFC might be associated with immobility behaviors in our study. Intriguingly, it has been suggested that despair consists of cognitive, emotional, behavioral, and biological domains in humans. Cognitive despair includes hopelessness, guilt, worthlessness and learned helplessness, while emotional despair comprises sadness, loneliness, anhedonia and apathy (Shanahan et al., 2019). However, the despair domain of immobility behavior in rodents during the TST or FST remains uncertain and requires further investigation and characterization.

The E/I balance in individual neurons affects input gating and controls the probability as well as timing of action potential firing (Bhatia et al., 2019). Our results suggest that the increase in the E/I ratio caused by disinhibition or BDNF-induced potentiation of excitatory synaptic transmission enhances hippocampal network activity and induces anti-despair-like behavior. DREADD-mediated manipulation of the activity in CA1 interneurons rapidly modified behavioral despair. Pharmacological suppression of inhibitory transmission by PTZ (20 mg/kg) treatment was sufficient to induce rapid anti-despair-like behaviors in both control

and stressed mice (Fig. 5). Interestingly, a previous study has shown that a low dose (1 mg/kg, i.p) of the $GABA_AR$ antagonist picrotoxin had no effect on immobility behaviors of mice during the FST (Autry et al., 2011). Consistent with this result, Betin et al. observed that oral administration of 10 mg/kg, but not 2.5 and 5 mg/kg picrotoxin produced a statistically significant reduction in the duration of immobility during the FST (Betin et al., 1982). Furthermore, sub-convulsant doses of bicuculine (a $GABA_AR$ antagonist) and strychnine (a glycine receptor antagonist) significantly reduced behavioral despair in mice (Betin et al., 1982). Thus, antagonists of inhibitory neurotransmission might have modified the E/I ratio in brain circuits through disinhibition and induced anti-despair-like behaviors.

Importantly, however, behavioral effects of PTZ did not last up to 48 h, despite a sustained activation of eEF2 at this time point. It should also be noted that PTZ-induced activation of eEF2 did not accompany BDNF elevation in the hippocampus. Considering the short half-life (2.5 – 3.8 h) of PTZ in the rodent brain (Meilleur et al., 2003), it is likely that the increased E/I ratio induced by disinhibition returned to the basal level after complete clearance of PTZ in the absence of BDNF-induced excitatory synaptic potentiation. RalBP1 mutant mice also displayed decreased despair-like behaviors and reduced p-eEF2 levels but normal BDNF levels. Reduced interneuron density might result in permanent modification of E/I ratio in CA1 pyramidal neurons and lead to stable anti-despair-like behavior in $RalBP1^{-/-}$ mice. Thus, increased E/I ratio seems sufficient and necessary for antidepressant behavior. Our results further suggest that dephosphorylation of eEF2 is not sufficient to induce elevation of BDNF levels but that it is associated with neuronal activity and/or E/I ratio.

In our study, ketamine (5 mg/kg) exhibited rapid (< 30 min) and sustained (~ 48 h) behavioral effects. Notably, ketamine rapidly decreases GABAergic synaptic transmission onto hippocampal CA1 pyramidal neurons (Widman and McMahon, 2018). Ketamine more effectively inhibits the NMDARs on GABAergic interneurons than those on pyramidal neurons, resulting in decreased firing of interneurons and subsequent bursting of pyramidal neurons (Homayoun and Moghaddam, 2007; Duman et al., 2016). These findings suggest that the rapid antidepressant effect of ketamine is attributable (either in full or in part) to the enhanced E/I ratio caused by disinhibition. In contrast to mice that received PTZ, which showed transient antidepressant activity, elevation of BDNF and activation of the downstream signaling

molecules ERK and mTOR were observed in hippocampus from ketamine-treated mice (Fig. 6). This indicates that the long-lasting antidepressant action of ketamine might originate from enhanced E/I ratio or increased signal to noise caused by BDNF-induced neurotropic and neuroplastic changes (Kang and Schuman, 1995; Ying et al., 2002; Alonso et al., 2004). Selective suppression of the sustained antidepressant effect of ketamine by the TrkB receptor antagonist ANA-12 further supports this finding (Fig. 6). Considering that BDNF signaling is normal in RalBP1$^{-/-}$ and PTZ-treated mice, the present study also indicates that disinhibition itself is not sufficient to induce BDNF elevation in hippocampus. Inhibition of NMDAR activity in addition to disinhibition might be required for BDNF elevation (Autry et al., 2011). However, the ketamine metabolite (2R,6R)-hydroxynorketamine (HNK), which exhibits acute and long-lasting antidepressant activity, elevates BDNF levels in the hippocampus through a NMDAR-independent mechanism (Zanos et al., 2016). A recent study reports that ketamine and (2R,6R)-HNK, but not the NMDAR antagonist MK-801, increases cyclic adenosine monophosphate (cAMP) -protein kinase A (PKA) signaling in astrocytes, leading to increased phosphorylation of cAMP response element-binding protein (CREB) and BDNF expression (Wray et al., 2018). Although the mechanisms underlying antidepressant-induced BDNF elevation are not fully understood, our results suggest that enhanced E/I ratio, either by disinhibition or by BDNF-induced synaptic modification, is critical for antidepressant responses.

Methods

Animals.

All experiments were performed with C57BL/6 male mice. Animals were group housed (3−5/cage) in a specific pathogen free facility and maintained in a climate-controlled room with free access to food and water in 12 h light/dark cycle. Generation and genotyping of RalBP1 mutant mice were described previously (Han et al., 2009; Bae et al., 2013). RalBP1 mutant mice and Vgat-ires-Cre (Slc32a1$^{tm2(cre)Lowl}$ knock-in; The Jackson Laboratory stock #016962) mice were backcrossed to C57BL/6 for at least 10 generations before use. Animal maintenance and all animal experiments were approved by the Institutional Animal Care and Use Committee (IACUC) at SNU.

Behaviors analyses

All behavioral tests were performed between 10 a.m. and 6 p.m. with male mice that were at least 9 weeks old at the start of testing. All experimental mice were acclimated to the behavior testing room for at least 1 h prior to beginning of testing. Between trials, mazes and apparatuses were cleaned with 70% ethanol. Muscimol, pentylenetetrazol and ANA-12 were purchased from Sigma-Aldrich (St. Louis, MO, USA). Ketamine hydrochloride was purchased from Yuhan (Seoul, Korea). Most of the behavioral tests were conducted as previously described (Bae et al., 2018), unless otherwise noted.

For tail suspension test (TST), mice were suspended by the tail from a metal hook extending from a steel bar using an adhesive tape in a 3-sided chamber with opaque walls. The distance between the floor of the chamber and the steel bar was approximately 40 cm. Mice that climbed onto their tail or fell off during the test were excluded from analysis. The duration of immobility over a 6-min session was manually scored by an experienced experimenter blind to treatment and mouse genotype.

Forced swim test (FST) was conducted by placing mice in glass beakers (20 cm high, 15 cm in diameter) containing 25−26 °C water at a 15-cm depth. An opaque plastic divider was placed between the glass beakers. Water was regularly changed and the beakers were cleaned between

subjects. A mouse was judged to be immobile when it remained floating in the water without struggling or swimming and was only making minimum movements necessary to stay afloat. The total duration of immobility over the 6 min observation period was scored by an experimenter blinded to the experimental details.

Sucrose preference test was performed once daily for 3 days. Mice were deprived of water but not food for 12 h before each test and allowed to freely access to both water and 1% sucrose in individual cages for 12 h. The position of each bottle was switched daily to avoid false sucrose preference resulting from side bias. Volume of liquid consumed was determined by weighting the bottles. The preference (%) for sucrose solution was calculated as follows: (sucrose solution intake /total liquid intake) × 100%.

Open field test was conducted by placing in the center of an open field apparatus with opaque walls (40 × 40 × 40 cm) in a dimly lit room. The behavior of each mouse was monitored for 30 min by video recording. The total distance traveled and time spent in the entire open field and in the center (20 × 20 cm) were calculated using video tracking software (Ethovision XT, Noldus, Netherlands).

Elevated plus maze test was performed using a plus-shaped maze with two open arms and closed arms surrounded by opaque walls (20 cm in height). The maze was elevated 50 cm from the floor, and dimension of each arm was 5 cm wide and 30 cm in length. Each mouse was place in the center of the maze and movement of the mouse was video recorded for 5 min.

The elevated zero maze consisted of black acrylic in a circular track 5 cm wide, 60 cm in diameter, and elevated 50 cm from the floor. The maze was divided into four equal quadrants, two of which were enclosed with black acrylic walls (20 cm in height). Each mouse was placed in the center of one of the two closed quadrants and movement of the mouse was video recorded for 5 min.

The chronic unpredictable stress (CUS) protocol has been described previously (Yoon et al., 2014). Mice were exposed in a random order to a variety of chronic stressors, including a wet cage (12 h), light-dark cycle reversal (24 h), white noise (100 dB, 12 h), cold water swim (10 °C, 1 h), restraint (2 h), cage shake (30 rpm, 12 h) and electric foot shocks (10 scrambled shocks with duration of 2 s over 120 min). Animals were subjected to one stressor daily for 28 days.

The Morris water maze test was performed using a white circular pool (120 cm in diameter) filled with 23°C–25°C water, which was made opaque with nontoxic white paint. A transparent circular platform (10 cm in diameter) submerged 1 cm beneath the surface. Two-day pre-training sessions consisted of one trial per day, and each mouse was allowed to remain on the visible platform for 30 s. The mice were then trained to find the hidden platform for 7 days with four trials per day and inter-trial intervals of 1 min. In each trial, mice were released at one of the three starting points and allowed to find a submerged platform. If mice did not locate the platform within 90 s, they were manually placed on the platform by the experimenter. Mice remained on the platform for 30 s before subsequent trials or before being returned to home cages. The probe test was performed 1 d after the completion of the training sessions. Swim paths and quadrant occupancies of each mouse were analyzed using video tracking software (Ethovision XT, Noldus).

The accelerating rotarod test was performed using the Rotamex 5 equipment (Columbus Instruments, OH, USA). Mice were placed on motionless rods, which were then accelerated from 5 to 40 rpm over 5 min. The latencies to falling off the rotating rod were measured. Each mouse was trained one daily for 3 days.

Training sessions for contextual and cued fear conditioning consisted of a 300 s exploration period (Pre-CS, contextual), followed by the presentation of an 18 s tone and a 2 s tone paired with a foot shock (0.7 mA) in the fear conditioning chamber (Coulbourn Instruments). Afterwards, each mouse was kept in the chamber for 60 s before being returned to its home cage. Contextual fear conditioning tests were performed in the same chamber (CS, contextual) 24 h after the training by monitoring mouse activity for 5 min. For cued fear conditioning, mice were placed in a distinct chamber, and their activities (pre-CS, cued) were monitored for 180 s, followed by presentation of a 180 s tone (CS, cued). The time spent freezing was scored post hoc by an experimenter blind to genotype.

Marble burying test was performed by placing animals individually in a transparent acrylic cage containing 15 clean glass marbles (1.5 cm in diameter) spaced evenly (3 × 5) on the surface of the 5-cm-deep bedding. Animals were allowed to explore the marbles for 10 min, and the number of marbles buried with bedding up to two-thirds of their surface area was counted.

Social behavior of animals was tested using the three-chambered social approach apparatus. The apparatus was white open-topped box (60 × 40 × 20 cm) and divided into three chambers (a 20-cm-wide center chamber and 20-cm-wide side chambers) with two acrylic walls. Each of the two side chambers contained an empty wire cup. Dividing walls had retractable doorways that allowed access into each chamber. During the habituation phase, animals were placed in the center chamber and allowed to explore freely for 10 min. During the sociability phase, the animal was gently guided to the center chamber, and the two doors were blocked while a stranger C57BL/6 mouse (stranger 1) placed inside one of the wire cups and an inanimate object was placed inside the other wire cup. Then, the two doors were opened and the subject animal was allowed to explore all the three chambers for 10 min. The amount of time spent in each chamber and time spent exploring mice or objects were measured. For the social novelty test, the subject mice again gently guided to the center chamber, and the two doors were blocked while an inanimate object was replaced by a novel unfamiliar mouse (stranger 2). Afterwards, the two doors were opened and the subject animal again allowed to explore all three chambers for 10 min. The behavior of the animals was recorded and analyzed using video tracking software (Ethovision XT, Noldus). All stranger mice were males of the same age and previously habituated to being enclosed in wire cups in the apparatus for 30 min one day before the test.

Pre-pulse inhibition (PPI) test was performed using the SR-Lab Startle Response system (San Diego Instruments, Ca, USA). Mice were placed into a small transparent tube mounted on a movement sensor platform in a sound-attenuating chamber and acclimated for 10 min before the testing session. The startle pulse was 120 dB (40 ms) and pre-pulses were either 75 or 80 dB (20 ms). During the acclimation period and each test session, background white noise (65 dB) was continuously presented. Baseline startle responses of animals were measured by 5−10 startle pulse (120 dB) alone trials, with inter-trial interval of 30 s. The peak startle amplitude was determined by measuring the largest positive and negative peaks of the startle response within a 300 ms window after the onset of the acoustic stimulus. During the PPI sessions, the same startle pulse preceded (100 ms) by a 75 dB or 80 dB pre-pulse in a pseudorandom order, with 5 testing trails per each pre-pulse. Scores for each measure were averaged, and PPI was calculated as a percent reduction of startle response: PPI (%) = (startle pulse alone – startle pulse with pre-pulse) / startle pulse alone) × 100.

Constructs and virus preparation

For Gabrg2 knockdown assay, Gabrg2 cDNA was amplified from mouse hippocampal cDNA and was cloned into pGW1 vector. Four independent shRNA (#1: gcattggaagctcagtctactctcctgta; #2: tggaatgatggtcgagttctctacacctt; #3: ccaaggtctcctatgtcacagcaatggat; #4: tggattgaggaatacaactgaagtagtga) constructs in the pGFP-V-RS vector and a non-targeting (NT: gcactaccagagctaactcagatagtact) pGFP-V-RS plasmid were purchased from OriGene (Cat. # TL515175). For lentivirus-mediated expression, the cassettes containing the human U6 (hU6) promoter-shRNA#3 and hU6-NT were amplified by PCR, and then subcloned into the pLVX-DsRed-Monomer-C1 (Clontech) vector, displacing the CMV promoter-DsRed-Monomer cassette. The PGK promoter-puromycin resistance gene cassette in the vector was further replaced by the CMV-eGFP cassette from the pEGFP-C1 vector (Clontech). The sequence-verified plasmid was transfected into Lenti-X 293T cells (Takara Bio) together with the packaging plasmid psPAX2 (Addgene) and the envelope plasmid pMD2.G (Addgene) using a polyethylenimine (PEI)-based transfection protocol (total DNA to PEI μg ratio of 1: 2). The ratio of pLVX-shRNA: psPAXs: pMD2.G was 4:1:2 (total 300 μg / 245 mm square dish). Lenti-X 293T cells were cultivated in the high glucose (4.5 g/L) Dulbecco's Modified Eagle's Medium (DMEM) containing 4 mM L-glutamine, 3.7 g/L sodium bicarbonate, 10% (v/v) tetracycline-free fetal bovine serum (FBS), 1 mM sodium pyruvate, and 1% (v/v) penicillin/streptomycin. The medium was replaced with fresh medium 24 h after transfection. Lentivirus-containing medium was harvested 72 h after transfection and was briefly centrifuged at 900 g for 10 min to remove debris. Supernatant was filtered (0.45-μm pore size) for sterilization, and lentivirus particles were concentrated by 2 rounds of ultracentrifugation (10,000 g for 2 h). Pellets were resuspended in PBS, aliquoted and stored at −80 °C. Viral titer (10^{12-13} IU/ml) was determined by transfecting serially diluted virus stocks into HEK293T cells and analyzing the number of GFP-positive cells using a fluorescence-activated cell sorter (FACS).

AAV2/hSyn-DIO-mCherry (#50459), AAV2/hSyn-DIO-hM3Dq-mCherry (#44361) and AAV2/hSyn-DIO-hM4Di-mCherry (# 44362) were obtained from Addgene (Watertown, MA, USA).

Surgery and stereotaxic injection

Under deep anesthesia with a mixture of Zoletil (50 mg/kg, i.p) and Xyalazine (1 mg/kg, i.p), mice were placed in a stereotaxic device. The skin was cut over the midline and craniotomies were performed bilaterally over the hippocampus. Either purified AAV (0.5 μl/side) or lentivirus (1 μl/side) was injected into the CA1 region of the dorsal medial hippocampus (−1.9 anteroposterior, ±1.5 mediolateral, −1.8 dorsoventral from the Bregma) using a Hamilton syringe at a rate of 100 nL/min. After completion of injection, the needle (33 gauge) was remained in place for an additional 10 min to allow the diffusion of the injection medium, and then carefully retracted to prevent backflow. Experiments were performed 3−4 weeks after viral injections.

For intrahippocampal infusion of muscimol, cannula assemblies consisted of a stainless-steel guide cannula (26 gauge with 2 mm) and a stylet were bilaterally implanted into the dorsal medial hippocampus (−1.9 anterior/posterior, ±1.5 medial/lateral, −1.2 dorsal/ventral) and were affixed to the skull with dental cement. Following surgery, mice were allowed to recover for at least 10 days before microinjection. Intrahippocampal infusion (0.5 μl/side) was made using a syringe pump (Harvard Apparatus, Pump 11) at a rate of 100 nL/min. Stainless steel injection cannulas connected to the injection syringe by polyethylene tubing were inserted into the guide cannulas. Following microinjection, the injection cannulas were remained in place for 5 min to allow diffusion of the solution into the tissue and then replaced by stylets.

Electrophysiology

Parasagittal hippocampal slices (400 μm thick) were prepared using a vibratome (Leica, Germany) in ice-cold dissection buffer (sucrose 230 mM; $NaHCO_3$ 25 mM; KCl 2.5 mM; NaH_2PO_4 1.25 mM; D-glucose 10 mM; Na-ascorbate 1.3 mM; $MgCl_2$ 3 mM; $CaCl_2$ 0.5 mM, pH 7.4 with 95% O_2/5% CO_2). The CA3 region was surgically removed immediately after sectioning. The slices were allowed to recover at 36 °C for 1 h in normal artificial cerebrospinal fluid (ACSF: NaCl 125 mM; $NaHCO_3$ 25 mM; KCl 2.5 mM; NaH_2PO_4 1.25 mM; D-glucose 10 mM; $MgCl_2$ 1.3 mM; $CaCl_2$ 2.5 mM, pH 7.4 with 95% O_2/5% CO_2), and then maintained

at room temperature.

All electrophysiological recordings were performed in a submerged recording chamber, which was perfused with heated (29–30°C) ACSF. The signals were filtered at 2.8 kHz and digitized at 10 kHz using a MultiClamp 700B amplifier and a Digidata 1440A interface (Molecular Devices, CA, USA). The data were analyzed by using custom macros written in Igor Pro (WaveMetrics, OR, USA).

To measure evoked EPSC/IPSC ratio, whole-cell voltage clamp recordings were made using patch pipettes (3–4 MΩ) filled with solution containing (in mM) 130 CsMeSO4, 10 TEA-Cl, 10 HEPES, 4 Mg-ATP, 0.3 Na-GTP, 5 QX-314-Cl and 10 EGTA, adjusted to pH 7.25 and 290 mOsm/kg. The synaptic responses were evoked at 0.05 Hz with an ACSF-filled broken glass pipette (0.3–0.5 MΩ) placed in the proximal region of the stratum radiatum. The mean AMPAR-mediated EPSCs were obtained by averaging 30–40 traces recorded at –57 mV. Stimulation intensity was adjusted to yield a 100–300 pA EPSC peak amplitude. To isolate the $GABA_AR$-mediated currents, 30–40 traces of synaptic currents were recorded at +3 mV. The series resistance and seal resistance were monitored, and the data were discarded if they changed by more than 20% during the recording.

The membrane potentials were recorded under whole-cell current clamp mode with a pipette solution containing (in mM) 110 K-gluconate, 20 KCl, 8 NaCl, 10 HEPES, 4 Mg-ATP, 0.3 Na-GTP, and 0.5 EGTA, adjusted to pH 7.25 and 290 mOsm/kg. Neurons displaying an unstable resting potential at the beginning or during the recording were discarded.

Miniature EPSCs (mEPSCs) were measured at –70 mV with a pipette solution containing (in mM) 110 K-gluconate, 20 KCl, 8 NaCl, 10 HEPES, 0.5 QX-314-Cl, 4 Mg-ATP, 0.3 Na-GTP, and 10 BAPTA, adjusted to pH 7.25 and 290 mOsm/kg. Spontaneous action potentials and IPSCs were blocked by tetrodotoxin (TTX, 1 μM) and picrotoxin (50 μM), respectively. For miniature IPSC (mIPSC) recording, K-gluconate in the pipette solution was replaced by equimolar KCl, and currents were measured at –70 mV in the presence of TTX (1 μM), NBQX (10 μM), and AP-5 (50 μM) in ACSF. The data were analyzed using custom macros written in Igor Pro (WaveMetrics). All reagents were purchased from Sigma-Aldrich (MO, USA), except for QX-314-Cl, CNO, NBQX, AP-5 from Tocris (Bristol, UK).

Immunohistochemistry and western blotting

Immunohistochemistry and western blotting analyses were performed as described previously (Bae et al., 2018). Briefly, mice were deeply anesthetized with diethyl ether and transcardially perfused with heparinized (10 U/ml) phosphate-buffered saline (PBS), followed by PBS-buffered 4% (w/v) paraformaldehyde (PFA). Brains were removed, post-fixed in 4% PFA for 48 h at 4 °C and cut into 60 μm coronal sections using a vibratome (VT1200S, Leica, Germany). The sections were post-fixed (1 h), permeabilized with 0.3% (v/v) Triton X-100 in PBS, incubated in blocking buffer (5% normal goat serum, 5% horse serum, 5% donkey serum, and 0.5% BSA in PBS) for 2 h. Sections were successively incubated with primary (anti-PV: Swant, Cat. # PV27; anti-SST: Santa Cruz Biotechnology, Cat. # sc-55565; anti-VIP: Immunostar, Cat. # 20077; anti-CCK: Abcam, Cat. # ab37274; anti-GAD67: Millipore, Cat. # MAB5406; anti-mCherry: Abcam, Cat. # ab167453; anti-GFP: Synaptic Systems, Cat. # 132 004; anti-NeuN: Millipore, Cat. # ABN78; overnight at 4 °C) and fluorescence (Cy3, Alexa fluor 647 or FITC: Jackson ImmunoResearch Laboratories, PA, USA) conjugated-secondary (3 h at room temperature) antibodies. Between each step, the sections were rinsed 3 times for 10 min with PBS. Images were acquired using a confocal laser scanning microscope (FV 3000, Olympus, Japan).

For western blotting, mouse hippocampi were homogenized in buffer (320 mM sucrose, 10 mM Tris-HCl, 5 mM EDTA, pH 7.4) containing phosphatase inhibitor cocktail (GenDEPOT, TX, USA, Cat. # P3200) and proteinase inhibitor cocktail (Sigma-Aldrich, MO, USA, Cat. # P8340). Proteins were separated by SDS-PAGE and transferred to nitrocellulose membranes. The membranes were successively incubated with primary and horseradish peroxidase (HRP)-conjugated secondary (Jackson ImmunoResearch Laboratories, PA, USA) antibodies. Signals were detected by enhanced chemiluminescence (GE Healthcare, UK) and quantified using MetaMorph software (Molecular Devices, CA, USA). The following primary antibodies were obtained from commercial suppliers: anti-ERK (Cat. # 9102S), anti-p-ERK (Cat. # 9106S), anti-eEF2 (Cat. # 2332S), anti-p-eEF2 (Cat. # 2331S), anti-mTOR (Cat. # 2972S), anti-p-mTOR (Cat. # 2971S) from Cell Signaling Technology; BDNF (Cat. # ab108319) from Abcam; Gabrg2 (Cat. # 224 003) from Synaptic Systems; tGFP (Cat. # TA150041) from Origene; α-tubulin (Cat. # T5168) from Sigma-Aldrich.

Statistical analysis

Statistical analyses were performed using Igor Pro (WaveMetrics) and SPSS (IBM, Armonk, USA). Normality of the collected data were determined by the Shapiro-Wilk test. The Mann-Whitney test was used to compare non-normally distributed samples. Samples satisfying normal distribution were compared using two-tailed Student's *t*-tests. For multiple groups, one-way ANOVA with Bonferroni post hoc test was used to compare samples. All bar graphs in the figures show the mean ± SEM. The levels of significance are indicated as follows: $^{*}p < 0.05$; $^{**}p < 0.01$; $^{***}p < 0.001$; n.s., not significant ($p \geq 0.05$). The number of cells, slices, or animals used for each experiment and statistical analysis are provided in Supplementary Table 1.

References

Ahrlund-Richter S, Xuan Y, van Lunteren JA, Kim H, Ortiz C, Pollak Dorocic I, Meletis K, Carlen M (2019) A whole-brain atlas of monosynaptic input targeting four different cell types in the medial prefrontal cortex of the mouse. Nat Neurosci 22:657-668.

Alonso M, Medina JH, Pozzo-Miller L (2004) ERK1/2 activation is necessary for BDNF to increase dendritic spine density in hippocampal CA1 pyramidal neurons. Learn Mem 11:172-178.

Aso E, Ozaita A, Valdizan EM, Ledent C, Pazos A, Maldonado R, Valverde O (2008) BDNF impairment in the hippocampus is related to enhanced despair behavior in CB1 knockout mice. J Neurochem 105:565-572.

Autry AE, Adachi M, Nosyreva E, Na ES, Los MF, Cheng PF, Kavalali ET, Monteggia LM (2011) NMDA receptor blockade at rest triggers rapid behavioural antidepressant responses. Nature 475:91-95.

Bae YS, Chung W, Han K, Park KY, Kim H, Kim E, Kim MH (2013) Down-regulation of RalBP1 expression reduces seizure threshold and synaptic inhibition in mice. Biochem Biophys Res Commun 433:175-180.

Bae YS, Yoon SH, Han JY, Woo J, Cho YS, Kwon SK, Bae YC, Kim D, Kim E, Kim MH (2018) Deficiency of aminopeptidase P1 causes behavioral hyperactivity, cognitive deficits, and hippocampal neurodegeneration. Genes Brain Behav 17:126-138.

Betin C, DeFeudis FV, Blavet N, Clostre F (1982) Further characterization of the behavioral despair test in mice: positive effects of convulsants. Physiol Behav 28:307-311.

Bhatia A, Moza S, Bhalla US (2019) Precise excitation-inhibition balance controls gain and timing in the hippocampus. Elife 8.

Cazorla M, Premont J, Mann A, Girard N, Kellendonk C, Rognan D (2011) Identification of a low-molecular weight TrkB antagonist with anxiolytic and antidepressant activity in mice. J Clin Invest 121:1846-1857.

Covington HE, 3rd, Lobo MK, Maze I, Vialou V, Hyman JM, Zaman S, LaPlant Q, Mouzon E, Ghose S, Tamminga CA, Neve RL, Deisseroth K, Nestler EJ (2010) Antidepressant effect of optogenetic stimulation of the medial prefrontal cortex. J Neurosci 30:16082-16090.

Duman RS, Monteggia LM (2006) A neurotrophic model for stress-related mood disorders. Biol Psychiatry 59:1116-1127.

Duman RS, Aghajanian GK, Sanacora G, Krystal JH (2016) Synaptic plasticity and depression: new insights from stress and rapid-acting antidepressants. Nat Med 22:238-249.

Essrich C, Lorez M, Benson JA, Fritschy JM, Luscher B (1998) Postsynaptic clustering of major GABAA receptor subtypes requires the gamma 2 subunit and gephyrin. Nat Neurosci 1:563-571.

Fanselow MS, Dong HW (2010) Are the dorsal and ventral hippocampus functionally distinct structures? Neuron 65:7-19.

Fischell J, Van Dyke AM, Kvarta MD, LeGates TA, Thompson SM (2015) Rapid Antidepressant Action and Restoration of Excitatory Synaptic Strength After Chronic Stress by Negative Modulators of Alpha5-Containing GABAA Receptors. Neuropsychopharmacology 40:2499-2509.

Goeldner C, Reiss D, Kieffer BL, Ouagazzal AM (2010) Endogenous nociceptin/orphanin-FQ in the dorsal hippocampus facilitates despair-related behavior. Hippocampus 20:911-916.

Han K, Kim MH, Seeburg D, Seo J, Verpelli C, Han S, Chung HS, Ko J, Lee HW, Kim K, Heo WD, Meyer T, Kim H, Sala C, Choi SY, Sheng M, Kim E (2009) Regulated RalBP1 binding to RalA and PSD-95 controls AMPA receptor endocytosis and LTD. PLoS Biol 7:e1000187.

Han Y, Heuermann RJ, Lyman KA, Fisher D, Ismail QA, Chetkovich DM (2017) HCN-channel dendritic targeting requires bipartite interaction with TRIP8b and regulates antidepressant-like behavioral effects. Mol Psychiatry 22:458-465.

Homayoun H, Moghaddam B (2007) NMDA receptor hypofunction produces opposite effects on prefrontal cortex interneurons and pyramidal neurons. J Neurosci 27:11496-11500.

Huang EJ, Reichardt LF (2001) Neurotrophins: roles in neuronal development and function. Annu Rev Neurosci 24:677-736.

Huang RQ, Bell-Horner CL, Dibas MI, Covey DF, Drewe JA, Dillon GH (2001) Pentylenetetrazole-induced inhibition of recombinant gamma-aminobutyric acid type A (GABA(A)) receptors: mechanism and site of action. J Pharmacol Exp Ther 298:986-995.

Jacob TC, Moss SJ, Jurd R (2008) GABA(A) receptor trafficking and its role in the dynamic modulation of neuronal inhibition. Nat Rev Neurosci 9:331-343.

Kang H, Schuman EM (1995) Long-lasting neurotrophin-induced enhancement of synaptic transmission in the adult hippocampus. Science 267:1658-1662.

Kim CS, Chang PY, Johnston D (2012) Enhancement of dorsal hippocampal activity by knockdown of HCN1 channels leads to anxiolytic- and antidepressant-like behaviors. Neuron 75:503-516.

Koike H, Fukumoto K, Iijima M, Chaki S (2013) Role of BDNF/TrkB signaling in antidepressant-like effects of a group II metabotropic glutamate receptor antagonist in animal models of depression. Behav Brain Res 238:48-52.

Kowianski P, Lietzau G, Czuba E, Waskow M, Steliga A, Morys J (2018) BDNF: A Key Factor with Multipotent Impact on Brain Signaling and Synaptic Plasticity. Cell Mol Neurobiol 38:579-593.

Kumar S, Black SJ, Hultman R, Szabo ST, DeMaio KD, Du J, Katz BM, Feng G, Covington HE, 3rd, Dzirasa K (2013) Cortical control of affective networks. J Neurosci 33:1116-1129.

Li N, Lee B, Liu RJ, Banasr M, Dwyer JM, Iwata M, Li XY, Aghajanian G, Duman RS (2010) mTOR-dependent synapse formation underlies the rapid antidepressant effects of NMDA antagonists. Science 329:959-964.

Marin O (2012) Interneuron dysfunction in psychiatric disorders. Nat Rev Neurosci 13:107-120.

Meilleur S, Aznavour N, Descarries L, Carmant L, Mamer OA, Psarropoulou C (2003) Pentylenetetrazol-induced seizures in immature rats provoke long-term changes in adult hippocampal cholinergic excitability. Epilepsia 44:507-517.

Mineur YS, Taylor SR, Picciotto MR (2014) Calcineurin downregulation in the amygdala is sufficient to induce anxiety-like and depression-like behaviors in C57BL/6J male mice. Biol Psychiatry 75:991-998.

Miyakawa T, Yamada M, Duttaroy A, Wess J (2001) Hyperactivity and intact hippocampus-dependent learning in mice lacking the M1 muscarinic acetylcholine receptor. J Neurosci 21:5239-5250.

Moser MB, Moser EI (1998) Functional differentiation in the hippocampus. Hippocampus

8:608-619.

Moy SS, Nadler JJ, Perez A, Barbaro RP, Johns JM, Magnuson TR, Piven J, Crawley JN (2004) Sociability and preference for social novelty in five inbred strains: an approach to assess autistic-like behavior in mice. Genes Brain Behav 3:287-302.

Nestler EJ, Barrot M, DiLeone RJ, Eisch AJ, Gold SJ, Monteggia LM (2002) Neurobiology of depression. Neuron 34:13-25.

O'Leary OF, Cryan JF (2014) A ventral view on antidepressant action: roles for adult hippocampal neurogenesis along the dorsoventral axis. Trends Pharmacol Sci 35:675-687.

Phillips JL, Norris S, Talbot J, Hatchard T, Ortiz A, Birmingham M, Owoeye O, Batten LA, Blier P (2019) Single and repeated ketamine infusions for reduction of suicidal ideation in treatment-resistant depression. Neuropsychopharmacology 45:606-612.

Porsolt RD, Bertin A, Jalfre M (1977) Behavioral despair in mice: a primary screening test for antidepressants. Arch Int Pharmacodyn Ther 229:327-336.

Przegalinski E, Tatarczynska E, Deren-Wesolek A, Chojnacka-Wojcik E (1997) Antidepressant-like effects of a partial agonist at strychnine-insensitive glycine receptors and a competitive NMDA receptor antagonist. Neuropharmacology 36:31-37.

Ren Z, Pribiag H, Jefferson SJ, Shorey M, Fuchs T, Stellwagen D, Luscher B (2016) Bidirectional Homeostatic Regulation of a Depression-Related Brain State by Gamma-Aminobutyric Acidergic Deficits and Ketamine Treatment. Biol Psychiatry 80:457-468.

Shanahan L, Hill SN, Gaydosh LM, Steinhoff A, Costello EJ, Dodge KA, Harris KM, Copeland WE (2019) Does Despair Really Kill? A Roadmap for an Evidence-Based Answer. Am J Public Health 109:854-858.

Shi HS, Zhu WL, Liu JF, Luo YX, Si JJ, Wang SJ, Xue YX, Ding ZB, Shi J, Lu L (2012) PI3K/Akt signaling pathway in the basolateral amygdala mediates the rapid antidepressant-like effects of trefoil factor 3. Neuropsychopharmacology 37:2671-2683.

Shirayama Y, Chen AC, Nakagawa S, Russell DS, Duman RS (2002) Brain-derived neurotrophic factor produces antidepressant effects in behavioral models of depression. J Neurosci 22:3251-3261.

Sik A, Penttonen M, Ylinen A, Buzsaki G (1995) Hippocampal CA1 interneurons: an in vivo intracellular labeling study. J Neurosci 15:6651-6665.

Snyder CR, Harris C, Anderson JR, Holleran SA, Irving LM, Sigmon ST, Yoshinobu L, Gibb J, Langelle C, Harney P (1991) The will and the ways: development and validation of an individual-differences measure of hope. J Pers Soc Psychol 60:570-585.

Steru L, Chermat R, Thierry B, Simon P (1985) The tail suspension test: a new method for screening antidepressants in mice. Psychopharmacology (Berl) 85:367-370.

Strange BA, Witter MP, Lein ES, Moser EI (2014) Functional organization of the hippocampal longitudinal axis. Nat Rev Neurosci 15:655-669.

Sutton MA, Taylor AM, Ito HT, Pham A, Schuman EM (2007) Postsynaptic decoding of neural activity: eEF2 as a biochemical sensor coupling miniature synaptic transmission to local protein synthesis. Neuron 55:648-661.

Swerdlow NR, Weber M, Qu Y, Light GA, Braff DL (2008) Realistic expectations of prepulse inhibition in translational models for schizophrenia research. Psychopharmacology (Berl) 199:331-388.

Thomas A, Burant A, Bui N, Graham D, Yuva-Paylor LA, Paylor R (2009) Marble burying reflects a repetitive and perseverative behavior more than novelty-induced anxiety. Psychopharmacology (Berl) 204:361-373.

Tricoire L, Pelkey KA, Erkkila BE, Jeffries BW, Yuan X, McBain CJ (2011) A blueprint for the spatiotemporal origins of mouse hippocampal interneuron diversity. J Neurosci 31:10948-10970.

Turecki G, Ernst C, Jollant F, Labonte B, Mechawar N (2012) The neurodevelopmental origins of suicidal behavior. Trends Neurosci 35:14-23.

Widman AJ, McMahon LL (2018) Disinhibition of CA1 pyramidal cells by low-dose ketamine and other antagonists with rapid antidepressant efficacy. Proc Natl Acad Sci U S A 115:E3007-E3016.

Wray NH, Schappi JM, Singh H, Senese NB, Rasenick MM (2018) NMDAR-independent, cAMP-dependent antidepressant actions of ketamine. Mol Psychiatry.

Xu W, Sudhof TC (2013) A neural circuit for memory specificity and generalization. Science 339:1290-1295.

Ying SW, Futter M, Rosenblum K, Webber MJ, Hunt SP, Bliss TV, Bramham CR (2002) Brain-derived neurotrophic factor induces long-term potentiation in intact adult hippocampus: requirement for ERK activation coupled to CREB and upregulation of Arc synthesis. J

Neurosci 22:1532-1540.
Yoon SH, Kim BH, Ye SK, Kim MH (2014) Chronic non-social stress affects depressive behaviors but not anxiety in mice. Korean J Physiol Pharmacol 18:263-268.
Zanos P, Thompson SM, Duman RS, Zarate CA, Jr., Gould TD (2018) Convergent Mechanisms Underlying Rapid Antidepressant Action. CNS Drugs 32:197-227.
Zanos P, Moaddel R, Morris PJ, Georgiou P, Fischell J, Elmer GI, Alkondon M, Yuan P, Pribut HJ, Singh NS, Dossou KS, Fang Y, Huang XP, Mayo CL, Wainer IW, Albuquerque EX, Thompson SM, Thomas CJ, Zarate CA, Jr., Gould TD (2016) NMDAR inhibition-independent antidepressant actions of ketamine metabolites. Nature 533:481-486.

Acknowledgements

S.H. Yoon, W.S. Song, and S.P. Oh are postgraduate students supported by Brain Korea 21 Plus Program. We thank the late Dr. Ronald S. Duman for critical reading of the manuscript and helpful comments. This study was supported by the National Research Foundation of Korea (NRF) grant funded by the Korea government (NRF-2017R1D1A1B03032935, 2018R1A5A2025964, and 2017M3C7A1029609), and by Creative-Pioneering Researchers Program through Seoul National University (SNU).

Author contribution

S.H.Y and M.-H.K conceived the project and designed the experiments. S.H.Y, S.W.S, and S.P.O performed experiments and analyzed the data. G.C and S.J.K conducted the cannula infusion experiments. S.H.Y and M.-H.K wrote the manuscript, with input from all other authors.